Journal of Power Sources 253 (2014) 17–26

Contents lists available at ScienceDirect

Journal of Power Sources

journal homepage: www.elsevier.com/locate/jpowsour

Fabrication of micro/nano-composite porous TiO_2 electrodes for quantum dot-sensitized solar cells

Xiaohui Song, Minqiang Wang*, Tiying Xing, Jianping Deng, Jijun Ding, Zhi Yang, Xiangyu Zhang

Electronic Materials Research Laboratory (EMRL), Key Laboratory of the Ministry of Education, International Center for Dielectric Research, Xi'an Jiaotong University, Xi'an 710049, China

HIGHLIGHTS

- PS spheres were added into TiO_2 paste to fabricate micro/nano-porous TiO_2 films.
- This structure avoids the unfavorable clogging of pores by aqueous colloidal QDs.
- The large pores created by burning PS enhance the scattering properties of the TiO_2 films.
- The influence of the added amount of PS on the photovoltaic properties was studied.
- A maximum efficiency of 2.23% was achieved with the optimal TiO_2/CdSe photoanode.

ARTICLE INFO

Article history:
Received 4 October 2013
Received in revised form
26 November 2013
Accepted 7 December 2013
Available online 18 December 2013

Keywords:
Titanium dioxide
Polystyrene sphere
Quantum dots-sensitized solar cell
Micro/nano-composite structure
Light scattering

ABSTRACT

For colloidal quantum dots-sensitized solar cells (QDSSC), the penetration and distribution of quantum dots (QDs) within electrodes is very crucial for performance improvement. In view of much bigger size of colloidal QDs than that of dye molecules, a TiO_2 electrode with open structure is helpful for the distribution of QDs. In this study, micro/nano-composite porous TiO_2 electrodes are fabricated by incorporating polystyrene (PS) spheres into the TiO_2 screen-printing paste. After sintering, the embedded PS spheres are burnt off, leaving randomly distributed submicrometer voids in the electrodes, which favor easy penetration of the colloidal CdSe QDs within the TiO_2 electrodes, and thus avoiding the unfavorable clogging of pores by CdSe QDs. In addition, this kind of composite structure enhances the scattering properties of the electrodes and hence the light capture inside the device. In order to obtain optimized devices, we probe into the influence of the PS concentration on the photovoltaic performance. The result shows that a maximum conversion efficiency of 2.23% is obtained for the QDSSC made from the PS:TiO_2 = 1:4 paste.

1. Introduction

Recently, quantum dot-sensitized solar cells (QDSSC) as a cost-effective alternative to silicon-based solar cells have attracted considerable attention and shown promise toward the development of next generation solar cells [1–5]. The configuration of a QDSSC is in close analogy to that of the dye-sensitized solar cells (DSSC), and the only difference is that QDSSC use the inorganic semiconductor QDs instead of molecular dyes as light absorbing material. The use of QDs as sensitizer has some several advantages over conventional dyes, such as high absorption coefficient and tunable band gap [6,7]. In addition, QDs open up new ways to generate multiple electron–hole pairs with a single photon through impact ionization [8–10], which could push the theoretical maximum conversion efficiency of QDSSC to 44% [11]. Although the conversion efficiencies of QDSSC still lag behind that obtained for DSSC [12], QDSSC are attracting increasing attention among researchers and are progressing very rapidly [13–15]. A record conversion efficiency of 6.5% has been achieved with perovskite $(CH_3NH_3)PbI_3$ QDSSC [16]. Moreover, the signature of multiple exciton generation has also been observed in PbS and PbSe QDSSC [17,18]. These achievements stress the potentiality of QDs in QDSSC configuration to produce low-cost and high-performing photovoltaic devices.

The reasons for the low power conversion efficiency of QDSSC are not yet clearly understood. One of the possible reasons is the difficulty of assembling sufficient QDs on a nanostructured TiO_2 electrode to obtain a well-covered QDs layer without pore-clogging

* Corresponding author. Tel./fax: +86 29 82668794.
E-mail addresses: song.sxh@stu.xjtu.edu.cn (X. Song), mqwang@mail.xjtu.edu.cn (M. Wang).

0378-7753/$ – see front matter
http://dx.doi.org/10.1016/j.jpowsour.2013.12.033

[19]. The architecture of TiO_2 electrodes is an important factor that determines the satisfactory assembly of QDs for improving the photovoltaic performance of QDSSC. Although many different TiO_2 electrode structures have been tested for use in DSSC, the significant differences between QDs and dyes make the most widely used TiO_2 electrode structure in DSSC unsuitable for highly efficient QDSSC. On the one hand, the sizes of organometallic dyes are generally below 1 nm, while the size of a QD with the addition of the capping molecules is in the range of 3–5 nm, or even higher [20,21]. Therefore, a limitation arises from the pore size of the nanostructured TiO_2 electrode. The pore sizes below 10 nm may hinder the penetration of QDs into the nanoporous structure, leading to a reduction of the amount of adsorbed QDs. Regarding the ideal TiO_2 electrode designed for DSSC, it generally consists of a porous film of interconnected TiO_2 nanoparticles (around 10–20 nm). These small nanoparticles provide a large surface area, which is one of the key points responsible for the high performance of DSSC, but lead to the formation of 5–15 nm pores, leading to serious difficulties for QDs penetration, which is deleterious for QDSSC performance [20]. Especially in the case of colloidal QDs, it has been show that practically 100% covering of flat TiO_2 surface can be attained but the covering area decreases dramatically to 14% when P25 TiO_2 nanostructured electrodes are employed [22,23]. On the other hand, QDs have a much higher extinction coefficient than conventional dyes [24]. This implies that the surface area of electrode in QDSSC may not need as much as those in DSSC. In fact, the use of a more open pore structures with lower surface area like nanowires [25,26], nanotubes [27], or inverse opals [28] in QDSSC have shown very promising results. Therefore, the architecture of TiO_2 electrodes for QDSSC is worth investigating so as to improve the distribution of QDs and thus enhance the performance of QDSSC.

In this paper, the architecture of TiO_2 electrode for QDSSC was optimized by incorporating monodispersed polystyrene (PS) latex particles into the P25 TiO_2 screen-printing paste. After sintering, these submicrometer sized PS spheres were burnt off, leaving behind randomly distributed submicrometer pores and three dimensional network of interconnected TiO_2 nanoparticles, and thus a modified TiO_2 electrode containing micro/nano-composite pores is obtained. These enlarged cavities could avoid the unfavorable clogging of pores by colloidal CdSe QDs during its deposition, resulting in uniform distribution of QDs throughout the TiO_2 electrode and an enhancement of the photovoltaic performance. In addition, the submicrometer pores gives the electrode the ability to scatter light, according to the Mie-theory [29]. Normally, to introduce such a light scattering effect, a scattering layer made of large TiO_2 particles is coated on top of the nanocrystalline TiO_2 layer. J. Yu et al. used 800–1000 nm TiO_2 hollow spheres as a top scattering layer to enhance light scattering [30–33], while L. Yang et al. electrosprayed polydispersed-size TiO_2 as scattering centers in the working electrode [34]. However, these double-layer configurations make the fabrication process more complex. The simple mechanical mixing method in our paper not only simplifies the fabrication process but also maintains similar light scattering. In order to obtain optimized devices, the influence of the added amount of PS on the photovoltaic properties was also studied.

2. Experimental

2.1. Synthesis of polystyrene spheres

Monodisperse PS latex spheres were synthesized by emulsifier-free emulsion copolymerization according to the literature using styrene as polymerized monomer, ammonium persulfate ($(NH4)_2S_2O_8$) as initiator, and methacrylic acid as functional monomer to provide carboxyl group on the surface of spheres [35]. Polymerization was conducted in a 250 ml reaction flask, placed in water bath, and refluxed under a N_2 atmosphere. 9 g styrene and 0.4 g methacrylic acid were mixed in a round-bottom flask, and 0.24 g $NaHCO_3$ dissolved in 80 ml of deionized water was added into the flask. The mixture was stirred for about 20 min and gradually heated to 60 °C. After that, 0.08 g of initiator $(NH4)_2S_2O_8$ in 20 ml water was added, and the reaction flask was heated to 75 °C. After the reaction of 24 h, the flask was removed from the water bath. For mixing with TiO_2 paste, PS spheres in this suspension were separated from the solvent by filtration, followed by rinsing with deionized water, redispersion and additional filtration. The collected powder was dried in air overnight.

2.2. Preparation of mixed PS–TiO_2 paste

The preparation of TiO_2 viscous pastes was carried out according to the literature [36]. It composed of TiO_2 nanoparticles (Degussa P25), α-terpineol as a solvent, 10% solution of ethyl cellulose in ethanol as a rheological agent, acetic acid as an aggregation blockers. The prepared TiO_2 colloid was used as the original and control paste, into which different amounts of PS spheres was added. The PS sphere were first diluted in 20 ml of ethanol and then mixed with prepared TiO_2 pastes with a weight ratio of PS:TiO_2 = 1:10, 1:4 and 1:2, respectively. The suspension was thoroughly mixed by an intensive sonication to break up any aggregates of nanoparticles and then stirred overnight at room temperature. After that the suspension was transferred to a beaker placed in a water bath and evaporated at 50 °C. After evaporating all ethanol in the solution, the mixed PS–TiO_2 paste formed.

The prepared PS embedded TiO_2 paste was then deposited on SnO_2:F coated conductive glass (15 Ω square^{-1}) by screen-printing method. This screen-printing procedure was repeated to adjust the thickness of the TiO_2 electrode. The as-prepared TiO_2 films were calcined in a muffle furnace at 500 °C for 1 h at heating speed of 2 °C min^{-1}. During sintering, PS spheres were burn out, leaving abundant cavities, whose sizes depend on the sizes of PS spheres. For the sake of comparison, a reference P25 TiO_2 electrode was also obtained in a similar way, however, without the addition of PS during its preparation. The area of the TiO_2 films was approximately 0.25 cm^2 (0.5 cm × 0.5 cm).

2.3. Fabrication of CdSe QDSSC

The preparation of CdSe QDs-sensitized TiO_2 (TiO_2/CdSe) photoanodes by the hydrothermal route has been described in detail elsewhere [37]. Briefly, by a molar ratio of 3:1, potassium borohydride (KBH_4) was used to react with selenium in water to prepare potassium hydrogen selenide (KHSe). Freshly prepared oxygen-free KHSe solutions was added to N_2-saturated $Cd(CH_3COO)_2$ solutions at pH 11.5 in the presence of thioglycolic acid (TGA). The molar ratio of Cd^{2+}:Se^{2-}:TGA was chosen as 1:0.1:3.6 in our experiments. 30 ml of the resulting CdSe precursor was transferred into a Teflon-lined stainless steel autoclave with a volume of 40 ml. Then the prepared TiO_2 electrodes were inserted into the autoclave, subsequently, the sealed autoclave was put into an oven and maintained at 160 °C for 15 h to promote the growth and assembly of CdSe QDs on TiO_2 electrodes. When the reaction finished, the autoclave was cooled to room temperature under flowing water, and the TiO_2/CdSe photoanodes were taken out, washed with deionized water to remove excess reactants, followed by drying in a N_2 flow. In this work, the TiO_2/CdSe photoanode made from pure P25 particle paste is named as photoanode 0, while the other TiO_2/CdSe photoanodes made from the mixed paste with the weight ratio of PS:TiO_2 = 1:10, 1:4, and 1:2 are referred to as photoanode 1, 2 and 3 for simplicity. To

increase the electron injection efficiency from CdSe QDs to TiO_2, annealing treatments were carried out in air at 400 °C for 360 s using a muffle furnace.

The QDSSC were prepared by sandwiching a TiO_2/CdSe photoanode and a Pt-coated FTO glass counter electrode using a 60-μm thickness Surlyn film. The internal space was filled with polysulfide electrolyte of 1 M Na_2S, 1 M S, and 0.1 M NaOH in water. The hole made on the counter electrode glass for injecting electrolyte was sealed by a Surlyn film and microscope cover glass.

2.4. Characterization methods

The morphology of the PS sphere, different TiO_2 electrodes and TiO_2/CdSe photoanodes were characterized by using an FEI Quanta 250 field emission gun scanning electron microscope. Transmission electron micrographs (TEM) of the samples were taken using a JEOL-2100 high-resolution transmission electron microscope (HRTEM). Before TEM characterization, aqueous colloidal CdSe QDs were precipitated from aqueous solution with an excess of 2-propanol and redispersed in ethanol, and TiO_2/CdSe composite film (photoanode 2) was scratched off from the glass substrates and dispersed in ethanol by sonication. TEM samples were prepared by dropping the CdSe QDs solution or TiO_2/CdSe composite suspension on the surface of carbon-coated copper grid and drying it in air. UV–Vis diffuse reflectance spectra was used to investigate light scattering ability of the TiO_2 electrodes (without QDs) and absorption spectra was used to investigate light harvesting property of the electrodes with QDs loaded. Both these two measurements were performed on a Jasco-V570 UV–Vis–NIR spectrophotometer equipped with an integrating sphere and $BaSO_4$ was used as a reference sample. Photovoltaic performances (*J–V* curves) of cell devices were recorded on a Keithley 2400 source meter under illumination by an AM 1.5 G solar simulator (Sciencetech Inc., SS-150). The power of the simulated light was calibrated to 100 mW cm^{-2} using a standard Si solar cell. The incident photon to current conversion efficiency (IPCE) was measured as a function of wavelength from 300 to 800 nm by using a model 7-SCSpec II system (Beijing 7-Star Optical Instruments Co., Ltd.).

3. Results and discussion

Polystyrene spheres are commonly used as colloidal templates because they are readily available in a wide range of size and easily removed by sintering. To improve the permeability of nano-structured TiO_2 electrodes, carboxyl stabilized PS spheres were introduced the TiO_2 electrodes, upon sintering these electrodes at 500 °C, the PS particles burn out thus leaving a reverse structure in the electrodes. The typical SEM photographs of the as-prepared PS spheres are shown in Fig. 1a, from which we can observe PS spheres prepared from emulsion polymerization are monodispersed. The average size of the PS spheres estimated from SEM photos is 240 nm. The micro/nano-composite porous TiO_2 electrodes were prepared through a simple mixing of submicrometer-sized PS spheres and nanosized P25 TiO_2 particles, followed by subsequent coating and calcinations on an FTO substrate, and the PS spheres vanish during the calcination process. Fig. 1b–i illustrates the

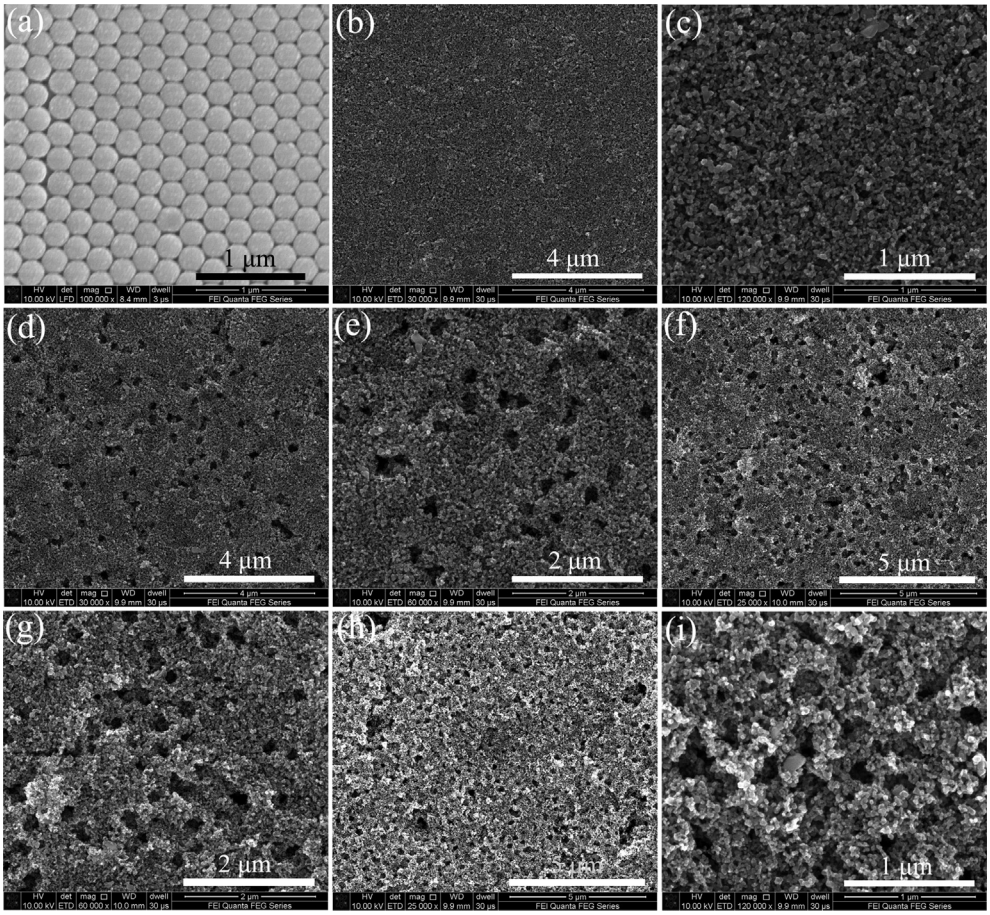

Fig. 1. Top-view FESEM images recorded at low and high magnification for (a) the PS spheres incorporated in TiO_2 screen-printing paste, and the TiO_2 electrodes made from: (b, c) pure TiO_2, (d, e) PS:TiO_2 = 1:10, (f, g) PS:TiO_2 = 1:4, and (h, i) PS:TiO_2 = 1:2 pastes.

top-view SEM images with low and high magnifications of the sintered TiO_2 electrodes with and without the application of PS spheres in the P25 TiO_2 paste. Without PS spheres, the surface of TiO_2 film appears to be very smooth and the film is a uniform network of TiO_2 nanoparticles with a size of approximately 20 nm, and the typical pore size of the TiO_2 layer is approximately 10 nm–20 nm (b–c). For the TiO_2 electrodes modified with PS sphere, PS evaporates, leaving abundant amounts of submicrometer cavities. These cavities are randomly arranged and more or less distributed uniformly on the TiO_2 surface. The size and density of the submicrocavities are determined by the dimension and concentration of the PS. The more PS was added to the paste, the more submicrocavities formed in TiO_2 electrodes. However, there was partial aggregation of PS spheres in the paste, hence some submicrocavities, especially in the higher PS content electrodes, are bigger than the original size of PS sphere.

Fig. 2 shows cross-sectional SEM micrograph of the TiO_2 electrode prepared from PS:TiO_2 = 1:4 paste. It can be seen that an 8.2 μm thick of TiO_2 film without crack formation was obtained. Abundant amounts of large cavities created by burnt PS spheres uniformly distributed throughout the entire TiO_2 cross-section, which indicates the PS sphere and TiO_2 nanoparticles dispersed homogeneously in ethanol. Due to the removal of PS and binder during the sintering, a little shrinkage of TiO_2 films occurs, resulting in the flattening of the large pore shape. This micro/nano-porous structure favors easy penetration of the relatively rigid and large colloidal QDs sensitizers into thick TiO_2 electrodes, avoiding the unfavorable clogging of pores by QDs during its deposition. These structure designed electrodes could support the diffusion of the electrolyte, particular those electrolytes with higher viscosity or the hole conducting polymers [38]. As discussed in previous report, these spherical voids in TiO_2 films can also act as scattering centers because these large pores could adjust the effective refractive index of the TiO_2 layer [39–41]. Therefore, the micro/nano-composite porous electrodes not only availed for the filling of QDs, but also may enhance light collection because of the strong light scattering.

Working electrodes made of TiO_2 nanoparticles for DSSCs appear semi-transparent, suggesting the transmittance of a portion of the visible light. An increase in the light scattering ability of the TiO_2 electrode is important for improving the light-harvesting efficiency and thus photon to current conversion efficiency of the resulting QDSSC. The amount of diffusely scattered light as a result of a beam of irradiation on the film can be quantified by diffuse reflectance spectroscopy. As a comparison, the diffuse reflection spectra of the TiO_2 films made from pure P25 nanoparticles paste was also measured (Fig. 3a). The P25 nanoporous TiO_2 film had relatively high diffuse reflection capacities in the wavelength range between 400 and 450 nm, while a rapid decrease in diffuse reflection capacities was observed for P25 film as the wavelength increased from 450 to 800 nm. After the PS sphere was added into the P25 paste, these PS modified TiO_2 films composed of interconnected TiO_2 nanoparticles and large cavities had higher diffuse reflection capabilities in the visible regions (from 400 to 800 nm), indicating that the incident light was significantly scattered within these micro/nano-composite porous TiO_2 electrodes. With the increase of PS content in P25 TiO_2 paste, the diffuse reflectance component increased gradually in the visible region and reached the maximum value at PS:TiO_2 = 1:2, meaning that light was scattered more strongly in these films compared to the standard P25 electrode. This phenomenon can be explained as follows: As described by Mie resonance theory [29], the scattering of light by spherical particles highly depends on the particle size and wavelength of the incident radiation, and the effective Mie scatters are those particles whose dimensions are comparable to the wavelength of light. The sizes of P25 nanoparticles are much smaller than the wavelength of visible light, therefore the pure P25 TiO_2 film exhibited the lowest reflectance. After the incorporation of PS sphere in P25 paste, the microcavities created by the decomposition of PS spheres have comparable size to the wavelength of visible light, and therefore these PS-modified electrodes would enhanced light scattering [39,42,43]. The multi-reflection between the TiO_2 matrix and air-filled pore can effectively enhance the optical path way of incident light. As a result, a higher diffuse reflection capability in visible regions is achieved. The high scattering effect will definitely increase the light harvesting efficiency of TiO_2/CdSe photoanode thus results in an enhanced photocurrent density for the QDSSC based on these photoanodes. The higher diffuse reflectance signifies that there was a very small amount of light passing through the film, explaining the opaque appearance of these films (shown in digital photographs Fig. 3c) in contrast to the semi-transparency of the standard P25 TiO_2 film, though they both contained 20 nm particles and have the same thickness. The transmittance data (see Fig. 3b) show a similar effect. The transmittance of the pure P25 TiO_2 electrode increased gradually from 400 to 800 nm, whereas the electrodes made from PS added P25 pastes had very low transmittance in the visible region, even for the PS:TiO_2 = 1:10 electrode. The low transmittance of the PS-modified TiO_2 electrodes suggests that the incident light is significantly blocked due to the strong scattering or reflection within these electrodes.

In order to clarify the influence of the TiO_2 structure on the performance of QDSSC, aqueous colloidal CdSe QDs were attached onto the four kinds of TiO_2 electrodes by linker-assisted hydrothermal method. This method integrates linker assisted assembly and in situ synthesis of colloidal QDs in a single step due to the use of bifunctional molecular linkers (TGA), which have been widely used to tether colloidal QDs to a wide gap nanostructured semiconductor electrode [44,45]. The TGA linkers exhibit a carboxylic group that attaches to TiO_2 and a thiol group that bind strongly to CdSe QDs through surface Cd^{2+} cations, so this sensitization

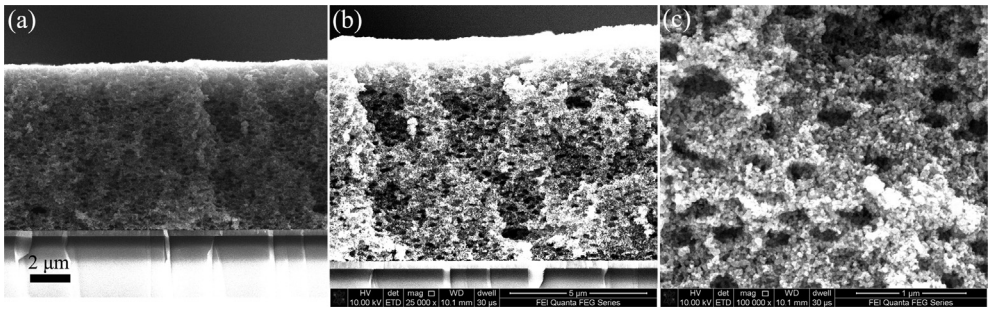

Fig. 2. Cross-sectional SEM images recorded at different magnifications for the micro/nano-composite porous TiO_2 electrode prepared from PS:TiO_2 = 1:4 paste.

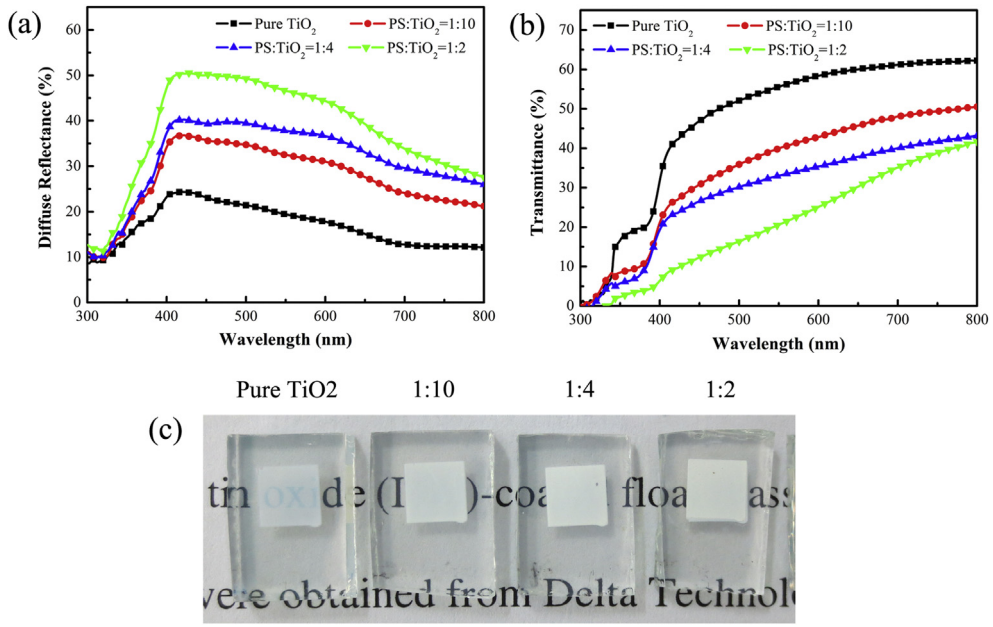

Fig. 3. Diffuse reflectance (a) and transmittance (b) spectra of the TiO_2 electrodes prepared from pure TiO_2 and mixed PS–TiO_2 pastes and the digital photographs (c) of the TiO_2 electrodes made from various pastes (screen-printed area is 0.5 cm × 0.5 cm).

strategy could achieve high sensitizer loading within TiO_2 electrodes. However, it is important to point out that, compared to the directly grown QDs with conventional successive ionic layer adsorption and reaction (SILAR) or chemical bath deposition (CBD) method, the aqueous colloidal CdSe QDs synthesized with this hydrothermal method have very good crystallinity, spherical shape and capped with TGA. Therefore, the size of QDs prepared with this method is usually larger than that of the flat QDs prepared with SILAR or CBD method. During the hydrothermal process, CdSe QDs grows gradually and simultaneously linked to the TiO_2 by means of several TGA molecular cables, which leads to the spatial separation between QDs and the TiO_2 electrode. In this case, the nano-sized pores of the pure P25 TiO_2 film are especially susceptible to clogging by CdSe QDs during deposition, and this phenomenon can clearly be observed in SEM images. Fig. 4a–d displays the top-view SEM micrographs of the TiO_2/CdSe photoanodes made from pure P25 TiO_2 (photoanode 0) and PS:TiO_2 = 1:4 paste. It can be seen that the incorporation of submicrometer pores in TiO_2 electrodes have a significant influence on the morphology of the as-prepared TiO_2/CdSe photoanodes. For the photoanode 0 (Fig. 4a), the nanochannels of P25 TiO_2 electrode are nearly completely blocked by accumulation of CdSe QD aggregates, and the nanoporous morphology of TiO_2 electrode are hard to be distinguish since the coverage of CdSe QDs on it, which would hinder the access of the electrolyte deep into the pores, leading to the detachment of hole-transport layers from TiO_2 electrodes. Therefore, this conventional P25 TiO_2 film is not a good candidate for efficient electrode of QDSSC. After proper amount of PS spheres were added into P25 TiO_2 paste, the morphology of the TiO_2/CdSe photoanode was greatly improved. The high concentration of PS latex gives rise to many submicrometer pores in the TiO_2 electrode, and these large pores make the TiO_2 channel more open and improve the permeability of the TiO_2 electrode, thus allowing the CdSe QD to enter the inner pores easily and distribute homogeneously within the TiO_2 electrode. This PS modification prevents the unfavorable clogging of pores by CdSe during its deposition, as it happened in the case of the electrode without modification. Looking at low-magnification SEM image (Fig. 4b), we can clearly discern the microporous structure created by PS sphere. Closer view at higher magnification (Fig. 4d) shows that the nanoporous structure formed by P25 TiO_2 nanoparticles is also retained after CdSe QDs deposition, implying that the electrolyte can well penetrate the photoanode. However, the average size of the pores decreased, which indicates a successful deposition of CdSe on the surface of the TiO_2. Subsequently, we used energy dispersive X-ray spectroscopy (EDS) to verify the existence of CdSe on TiO_2 electrode, and the EDS data for photoanode 2 was shown in Fig. 4c. Cd, Se and S elements appear after hydrothermal reaction, indicating that CdSe QDs have been successfully assembled onto TiO_2 surface, and the S element comes from TGA linker.

One important question from the standpoint of practical application of TiO_2/CdSe photoanode is the uniformity of the CdSe QDs distribution within the TiO_2 electrode. To obtain more detailed information about the QDs' distribution, chemical analysis is performed on cross section of the TiO_2/CdSe photoanode made from PS:TiO_2 = 1:4 paste using EDS. The cross-sectional SEM image of this photoanode is shown in Fig. 5a, and the results of the EDS elemental analysis are shown in Fig. 5b. It can be seen that the concentration of Cd and Se atoms keep at a nearly constant value throughout the entire TiO_2 cross-section, which indicates that the colloidal CdSe QDs not only penetrate all the way to the interface between TiO_2 and FTO, but they are also uniformly distributed across the TiO_2 electrode. The effective penetration of the CdSe across this micro/nano-composite porous TiO_2 electrode can also be observed through the naked eye, as there is no observable coloration difference between the front and back sides of the TiO_2/CdSe photoanode as shown in the inset of Fig. 5a.

Fig. 6a shows TEM images of as-synthesized aqueous colloidal CdSe QDs in autoclave. It can be seen that the TGA-capped CdSe QDs appeared as spherical particles with good monodispersity. As shown in the TEM image, the CdSe QDs had a mean diameter of about 4 nm, with the existence of well-resolved lattice planes showing that the aqueous CdSe QDs possessed a highly crystalline structure. To observe morphology of the TiO_2/CdSe photoanode in detail, we analyzed TEM image of the CdSe QDs-sensitized TiO_2 photoanode made from PS:TiO_2 = 1:4 paste. As shown in Fig. 6b, a

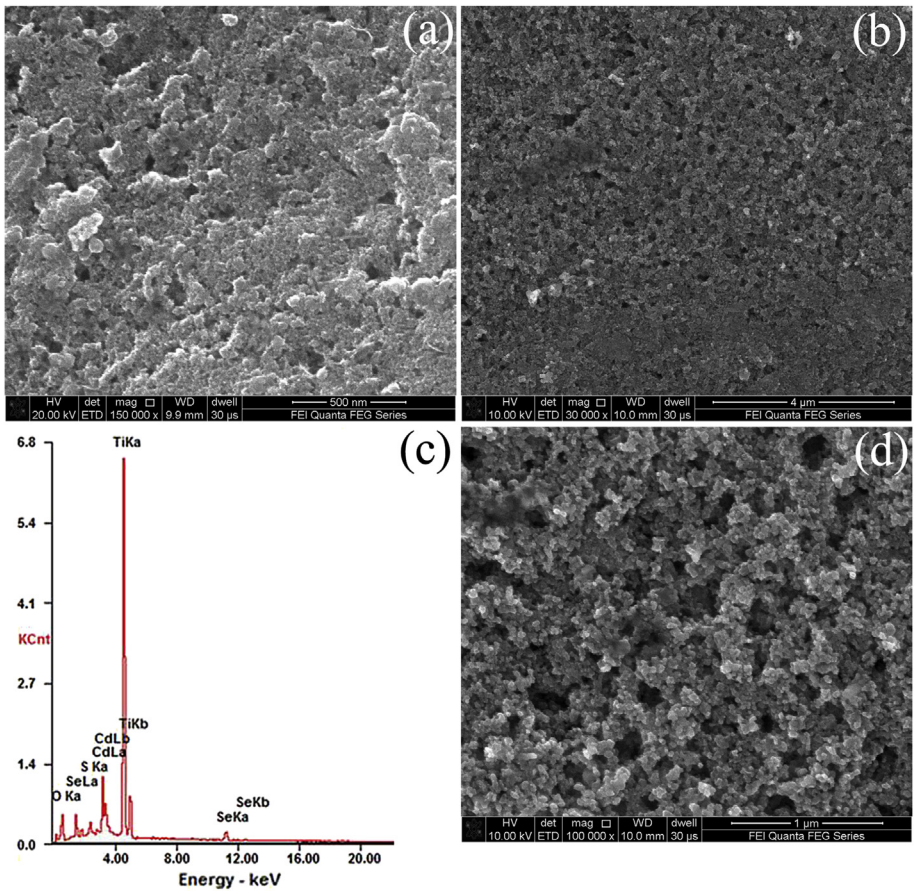

Fig. 4. The FESEM images of the TiO_2/CdSe photoanodes made from pure P25 TiO_2 nanoparticles paste (a) and PS:TiO_2 = 1:4 paste under different magnifications (b and d). (c) The EDS spectra of the TiO_2/CdSe photoanode shown in panel b.

number of CdSe QDs (black dots) can be clearly observed, randomly distributed over the TiO_2 surface.

Fig. 7a and b shows the optical absorption and diffuse transmission spectra of different TiO_2/CdSe photoanodes, and the absorption and transmittance spectrum of the bare TiO_2 film made form pure P25 paste is also shown for comparison. After hydrothermal treatment, all of white TiO_2 electrodes become homogeneously red in color (in the web version), as seen in Fig. 7c, confirming CdSe QDs deposition had taken place. Relative to the absorption edge of the bare TiO_2 electrode near 400 nm, the absorption edge of the TiO_2/CdSe photoanodes was extended to around 620 nm. As shown in Fig. 7a, the optical absorption of TiO_2/CdSe photoanodes with submicrocavities is enhanced, especially in the long-wavelength region, compared to that of photoanode 0. This enhancement can be attributed to the increase of the optical path through multiple scatterings of light in the submicrocavities [46]. Increased light absorption contributed to the increased photocurrent, thus increasing efficiency of the QDSSC. In addition, we noticed that the absorbance of TiO_2/CdSe photoanodes with submicrocavities show obvious red-shift as compared to that of photoanode 0, which can be ascribed to the contribution of submicrometer pores in TiO_2 electrode. For the pure P25 TiO_2 electrode, the nano-sized pores are especially susceptible to clogging by the accumulation of colloidal CdSe QD, as shown in Fig. 4a. Therefore, the size of CdSe QDs will be limited by the small pores. However, after PS was added into TiO_2 paste, the submicrometer voids created by burning PS enlarge the nanopores of TiO_2 and provide enough space to accommodate the colloidal CdSe QDs, thus allowing the CdSe QD to grow freely during hydrothermal reaction. In this case, the CdSe QDs deposited on these submicrometer pores will have bigger size than those loaded on pure P25 electrode. The more PS was added to the paste, the more amount of bigger sized CdSe in TiO_2 electrode, resulting in the gradual red-shift of the absorbance of the TiO_2/CdSe photoanodes with submicrocavities relative to that of the photoanode 0. The transmittance data in Fig. 7b shows a similar effect. In the long wavelength range (620–800 nm), the photoanode 0 shows a relatively high transmittance about 55%, while a dramatic decrease in transmission was observed for the TiO_2/CdSe photoanodes with submicrometer pores. The low transmittance confirms the superior light scattering properties of the submicrometer pores in TiO_2 electrode in the long wavelength region, which is also in good agreement with the diffuse reflection and transmittance results in Fig. 3.

To investigate the photovoltaic performance of the as-prepared TiO_2/CdSe photoanodes, sandwich-type thin layer cells were fabricated with platinized FTO as the cathode, and a polysulfide electrolyte as the hole transporter. The J–V curves corresponding to cell devices based on different photoanodes are shown in Fig. 8a, and the photovoltaic parameters including short circuit current density (J_{SC}), open circuit voltage (V_{OC}), fill factor (FF), and power conversion efficiency (η) are summarized in Table 1. According to the data shown in Table 1, the QDSSC made from pure P25 TiO_2 paste gives a J_{SC} of 7.48 mA cm^{-2}, a V_{OC} of 0.56 V, and an FF of 31%, yielding a power conversion efficiency of 1.31%. With the addition of PS sphere in P25 paste, the FF and the cell efficiency increased to 41% and 1.53% for PS:TiO_2 = 1:10, and 44% and 2.23% for PS:TiO_2 = 1:4, respectively. Comparing the FESEM images, absorption spectrum, and the photochemical response of the three

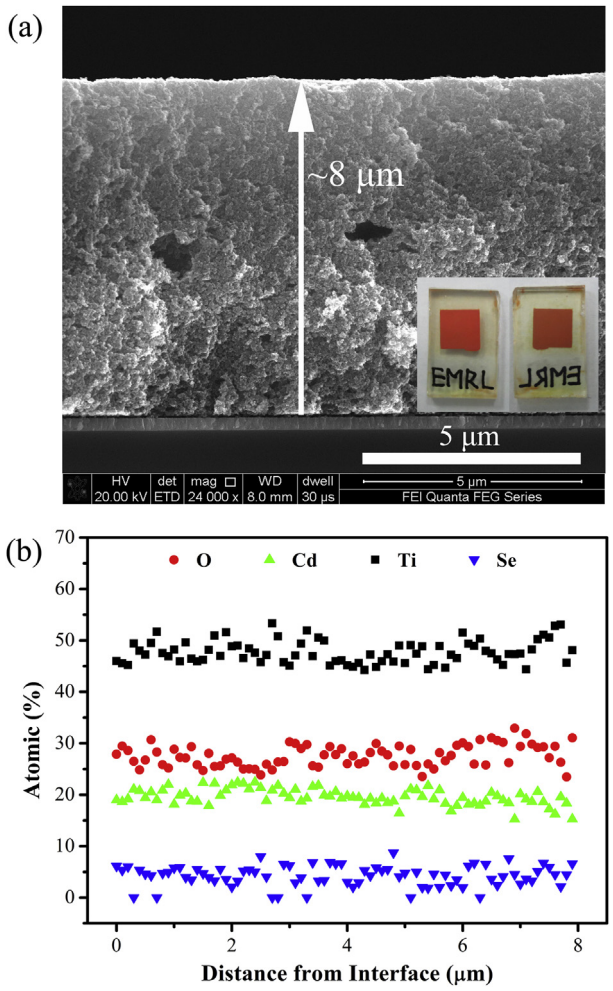

Fig. 5. (a) Cross-sectional SEM image of the TiO_2/CdSe photoanode made from PS:TiO_2 = 1:4 paste (TiO_2 film thickness, ~8 μm). The white arrow indicates the direction of the EDS scan shown in panel b. The inset shows digital images of the front and back of TiO_2/CdSe photoanode. (b) EDS analysis of the TiO_2/CdSe photoanode shown in panel a. The EDS spectra for each element were taken with respect to the FTO/TiO_2 interface (zero point on the abscissa).

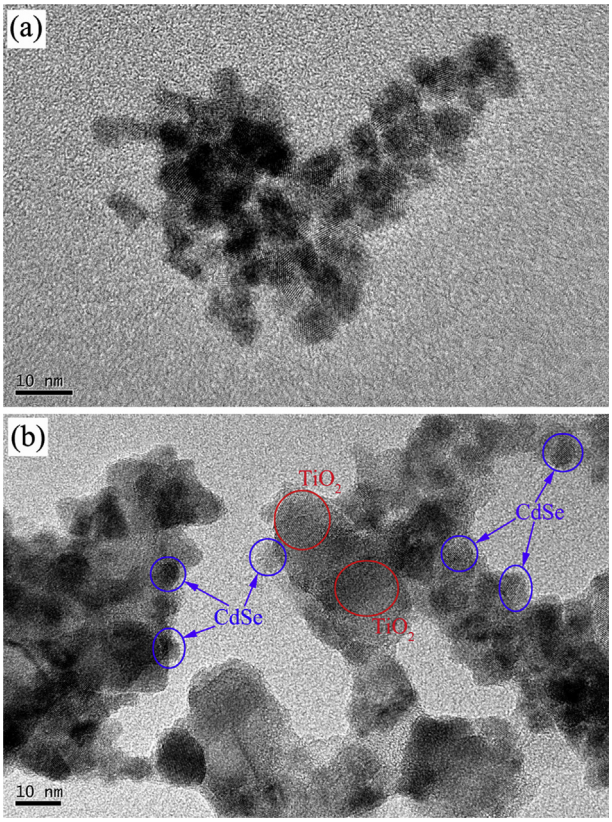

Fig. 6. (a) TEM image of the as-prepared CdSe colloidal QDs grown at 160 °C for 15 h. (b) TEM image of TiO_2 nanoparticles sensitized with CdSe QDs (photoanode 2).

photoanodes, it is clear that the improvement in the solar cell performance is mainly due to the improved morphology and microstructure caused by the addition of PS sphere in TiO_2 film. For the photoanode 0, the significant pore clogging inhibits the intimate contact of electrolyte and CdSe QDs, which delays the sensitizers from regeneration and increases the charge recombination rate in the CdSe QDs and thus reduces the fill factor and deteriorates the cell performance. The fill factor is a measure which reflects the increase in recombination or decrease in photocurrent with increasing photovoltage. Based on the foregoing discussion, one can infer that the recombination rate of photoelectron decreased after the incorporation of large pores. For photoelectrode 2, the micro/nano-composite porous structure has apparently prevented unfavorable clogging of pores by CdSe during its deposition, as it happened in the case of the photoelectrode 0, enabling formation of a more conformal CdSe/TiO_2 junction. This structure permits an efficient electrolyte penetrating and enables intimate contact of electrolyte and CdSe QDs, so the oxidized CdSe QDs can be quickly reduced to the initial state by receiving electrons from electrolyte, which reduces the charge recombination and results in a higher fill factor. Moreover, the multiple scattering of light in the submicrometer cavity increased the optical path, thus improving light absorption by the CdSe QDs, thereby increasing the photocurrent and the cell efficiency. As a result, a conversion efficiency of 2.23% was obtained which was 70% higher than that of the photoanode 0 (1.31%). However, when the weight ratio of PS to TiO_2 further increased to 1:2, the current density and conversion efficiency were largely reduced, as shown in Table 1. After superfluous PS spheres were introduced into the P25 TiO_2 paste, the screen-printed TiO_2 films did not have enough mechanical strength to retain the integrity of the porous structure after calcinations. Although the surface morphology of photoanode 3 is significantly improved compare to that of photoanode 0, the surface depression and poor adhesion of the TiO_2 film to FTO substrate directly lead to the decreased efficiency. Optimized amounts of PS sphere additions was thus set at PS:TiO_2 = 1:4 in the present study.

Although the conversion efficiencies obtained by micro/nano-composite electrodes do not attain those of that reported by P.V. Kamat and Y. Lin et al. [47,48], we believe that there is enormous scope for further improvement by optimizing the counter electrode, QDs sensitizer, and deposition process. For example, replacing Pt counter electrode with Cu_2S or PbS, using CdTe or CdSe/CdS QDs instead of CdSe as sensitizer, and ZnS post treatment et al. all will contribute to the improvement of the photovoltaic performance.

Fig. 8b displays the comparison of IPCE curves of the QDSSC made from pure TiO_2 and PS:TiO_2 = 1:4 pastes. As observed, the IPCE spectra adhere well to the shape of the absorption spectrum of the TiO_2/CdSe photoanodes shown in Fig. 7, indicating that most of the absorbed light by QDs is involved in the photocurrent generation. In the wavelength range of 330–650 nm, the QDSSC made from PS:TiO_2 = 1:4 paste exhibits a higher IPCE than the cell made from pure TiO_2, which correlate well with the increased photocurrent density for the former. It is well known that IPCE was dominated by

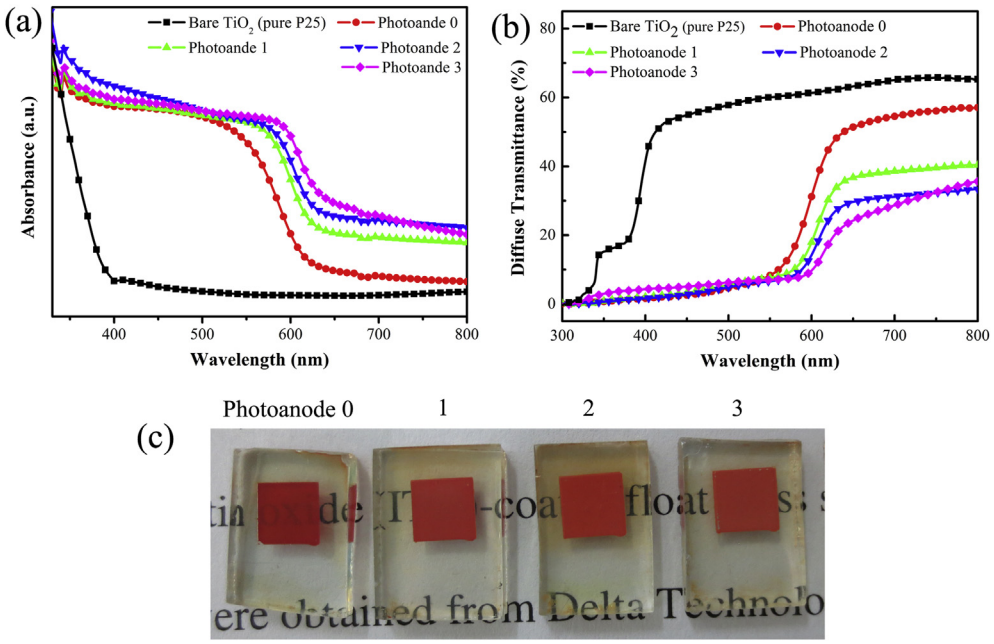

Fig. 7. Optical absorption (a) and diffuse transmittance (b) spectra of the TiO_2/CdSe photoanodes prepared from pure TiO_2 nanoparticles and mixed PS–TiO_2 pastes with different mass ratios of PS to TiO_2. The absorption and transmittance spectrum of the bare TiO_2 film is also shown for comparison. (c) Digital photographs of the TiO_2/CdSe photoanodes made from pure TiO_2 and different PS–TiO_2 pastes.

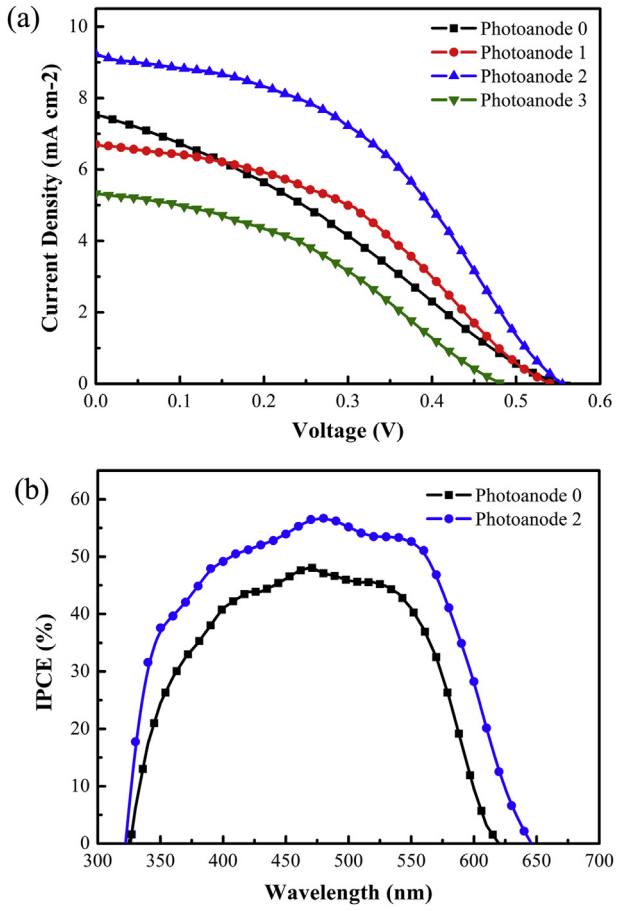

Fig. 8. (a) Current density–voltage (J–V) curves of QDSSC made from pure P25 TiO_2 and PS-incorporated pastes with weight ratio of PS:TiO_2 = 1:10, 1:4, and 1:2. (b) IPCE of QDSSC made from pure P25 TiO_2 and PS:TiO_2 = 1:4 paste.

$$\mathrm{IPCE}(\lambda) = \mathrm{LHE}(\lambda)\phi_{\mathrm{inj}}\eta_{\mathrm{EC}} \quad (1)$$

where LHE(λ) is the light-harvesting efficiency, ϕ_{inj} is the electron injection yield from the excited state of QDs into the TiO_2, and η_{EC} is the photogenerated electron collection efficiency at the FTO glass [49]. As discussed above, the blockage of TiO_2 nanochannels by accumulation of QDs aggregates leads to a severe drop in the IPCE. Since the extraction of holes to the electrolyte does not occur, recombination is enhanced. For the photoanode made from PS:TiO_2 = 1:4 paste, the good contact between QDs and electrolyte retards photogenerated electron–hole recombination and thus promotes the charge separation process. Furthermore, the enhanced light-scattering effect results in the improvement of the light-harvesting efficiency. As a result, photoanode 2 improves IPCE in the visible region and hence high plateau photocurrents are obtained. According to these results, one can conclude that the better infiltration of QDs and strong light scattering ability make the micro/nano-composite porous TiO_2 electrode as good candidate for fabricating efficient QDSSC.

The photoresponse of the QDSSC made from PS:TiO_2 = 1:4 paste was tested under periodic on–off one-sun illumination in the presence of the polysulfide electrolyte. The short circuit current density of the cell was measured as a function of time with shuttered light at 30 s intervals (Fig. 9). Under illumination with light, a prompt and stable photocurrent density of 9.23 mA cm^{-2} was obtained. This result implies that the photogenerated electron in CdSe

Table 1
Photovoltaic parameters obtained from the J–V curves of the QDSSC constructed using different TiO_2/CdSe photoanodes.

Samples	V_{OC} (V)	J_{SC} (mA cm^{-2})	FF (%)	η (%)
Photoanode 0	0.56	7.48	31.27	1.31
Photoanode 1	0.55	6.71	41.46	1.53
Photoanode 2	0.55	9.23	43.93	2.23
Photoanode 3	0.48	5.32	38.38	0.98

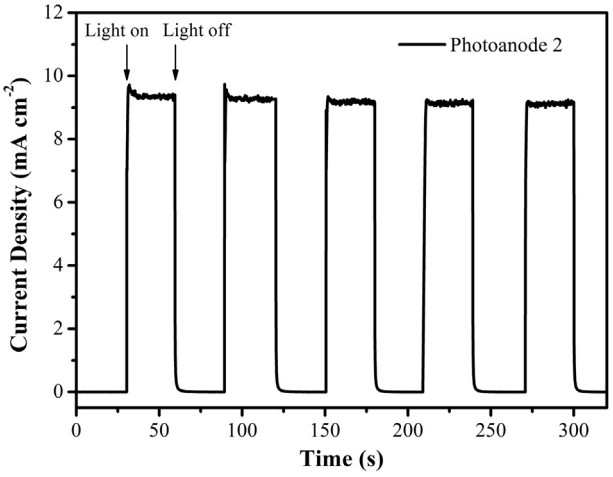

Fig. 9. Photocurrent response of QDSSC made from mixed PS:TiO_2 = 1:4 paste at 100 mW cm^{-2} with on and off cycles.

QDs can be rapidly transferred from CdSe QDs to TiO_2 substrate after annealing treatment, which effectively prevents the recombination of electron–hole pairs.

In order to understand the effect of photoanode structures on the electron lifetime, an open-circuit voltage decay (OCVD) measurement was carried out. The OCVD technique is a newly developing method which monitors the variation of V_{OC} with time for the cells illuminated to a steady state voltage, with subsequent interruption of illumination [49–51]. Under open circuit conditions with constant illumination, the equilibrium between electron accumulation and loss is established. Immediately upon termination of the illumination, open circuit voltage begins to decay because of the dominant recombination of accumulated electrons in TiO_2 with photogenerated holes or oxidized form of the redox couple. Therefore, the recombination rate of photoelectron is proportional to the rate of photovoltage decay, and the electrons lifetime τ_e at different voltage can be deduced from the V_{OC} decay curves according to the following relation [50]:

$$\tau_e = -\frac{k_{BT}}{e}\left[\frac{dV_{OC}}{dt}\right]^{-1} \quad (2)$$

where k_{BT}, e, and dV_{OC}/dt are the thermal energy, the positive elementary charge, and the derivative of the open circuit voltage transient, respectively. Fig. 10a shows the variation of V_{OC} with time for the cells made from pure TiO_2 and PS:TiO_2 = 1:4 pastes. It was observed that the V_{OC} decay rate decreased after the incorporation of submicrometer pores in TiO_2 electrode, revealing that the improved microstructure of TiO_2 inhibits the interfacial recombination. By applying Equation (2), the electron lifetime (in a log representation) as a function of V_{OC} was plotted in Fig. 10b. It is evident that the electron lifetime of the cells increases with decreasing V_{OC}. At the same V_{OC} values, the electron lifetimes of the cell made from PS:TiO_2 = 1:4 paste is longer than that of QDSSC made from pure TiO_2. The longer lifetime confirms that the successive scavenging of holes from quantum dots to electrolyte retards the interfacial recombination between electrons in the conduction band of TiO_2 and holes in quantum dots.

4. Conclusion

A serious of micro/nano-composite porous TiO_2 electrodes are prepared by mixing P25 TiO_2 paste with PS latex particles, and are applied to colloidal QDSSC successfully. Upon sintering these

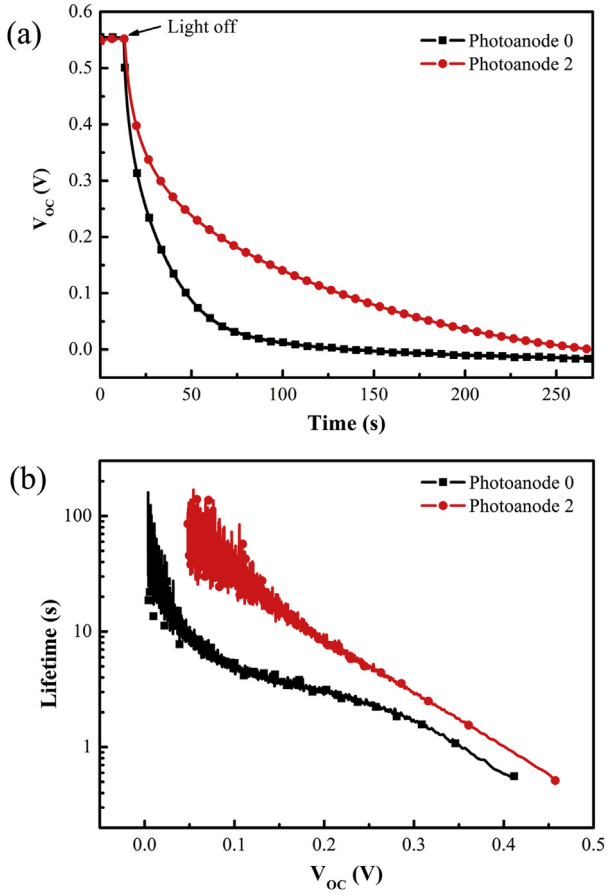

Fig. 10. (a) V_{OC} decay curves of the QDSSC made from pure P25 TiO_2 and PS:TiO_2 = 1:4 paste recorded during the relaxation from illuminated quasi-equilibrium to the dark. (b) The lifetime of electrons obtained from V_{OC} decay measurements.

electrodes at 500 °C, the submicrometer cavities created by burning PS make the TiO_2 channel more open, thus preventing the pore-clogging by CdSe QDs, as it happened in the case of the electrode without PS modification. Therefore, this micro/nano-porous structure reduces the charge recombination in colloidal QDSSC and results in a high fill factor. Furthermore, the light scattering in these submicrometer voids enhance the CdSe QDs absorption, thereby increasing the photocurrent and cell efficiency. With proper amount of PS sphere in P25 TiO_2 paste (PS:TiO_2 = 1:4), a conversion efficiency of 2.23% is obtained which is 70% higher than that of the pure P25 TiO_2 electrode (1.31%). However, further increasing the PS content causes the surface depression and poor adhesion of the TiO_2 electrode to FTO substrate, and thus decreasing the cell efficiency.

Acknowledgments

The authors gratefully acknowledge financial support from Natural Science Foundation of China (Grant Nos. 61176056 and 91123019). This work has been financially supported by the International Collaboration Program and the “13115” Innovation Engineering Project of Shaanxi Province (Grant Nos. 2013KW-12-05 and 2010ZDKG-58) and by the open projects from Institute of Photonics and Photo-Technology, Provincial Key Laboratory of Photoelectronic Technology, Northwest University, China.

References

[1] J.-W. Lee, D.-Y. Son, T.K. Ahn, H.-W. Shin, I.Y. Kim, S.-J. Hwang, M.J. Ko, S. Sul, H. Han, N.-G. Park, Sci. Rep. 3 (2013) 1050.

[2] X. Song, M. Wang, J. Deng, Z. Yang, C. Ran, X. Zhang, Xi Yao, ACS Appl. Mater. Interfaces 5 (2013) 5139–5148.
[3] J. Deng, M. Wang, X. Song, Y. Shi, X. Zhang, J. Colloid Interface Sci. 388 (2012) 118–122.
[4] H. Chen, L. Zhu, H. Liu, W. Li, J. Power Sources 245 (2014) 406–410.
[5] X. Song, M. Wang, H. Zhang, J. Deng, Z. Yang, C. Ran, X. Yao, Electrochim. Acta 108 (2013) 449–457.
[6] D.F. Underwood, T. Kippeny, S.J. Rosenthal, Eur. Phys. J. D 16 (2001) 241–244.
[7] Z. Lin, M. Wang, L. Zhang, Y. Xue, X. Yao, H. Cheng, J. Bai, J. Mater. Chem. 22 (2012) 9082–9085.
[8] R.D. Schaller, M. Sykora, J.M. Pietryga, V.I. Klimov, Nano Lett. 6 (2006) 424–429.
[9] M.T. Trinh, A.J. Houtepen, J.M. Schins, T. Hanrath, J. Piris, W. Knulst, A.P.L.M. Goossens, L.D.A. Siebbeles, Nano Lett. 8 (2008) 1713–1718.
[10] A.J. Nozik, Chem. Phys. Lett. 457 (2008) 3–11.
[11] M.C. Hanna, A.J. Nozik, J. Appl. Phys. 100 (2006) 074510.
[12] A. Yella, H.-W. Lee, H.N. Tsao, C. Y, A.K. Chandiran, M.K. Nazeeruddin, E.W.-G. Diau, C.-Y. Yeh, S.M. Zakeeruddin, M. Grätzel, Science 334 (2011) 629–635.
[13] T.-L. Li, Y.-L. Lee, H. Teng, Energy Environ. Sci. 5 (2012) 5315–5324.
[14] P.K. Santra, P.V. Kamat, J. Am. Chem. Soc. 134 (2012) 2508–2511.
[15] Z. Pan, K. Zhao, J. Wang, H. Zhang, Y. Feng, X. Zhong, ACS Nano 7 (2013) 5215–5222.
[16] J.-H. Im, C.-R. Lee, J.-W. Lee, S.-W. Park, N.-G. Park, Nanoscale 3 (2011) 4088–4093.
[17] J.B. Sambur, T. Novet, B.A. Parkinson, Science 330 (2010) 63–66.
[18] O.E. Semonin, J.M. Luther, S. Choi, H.-Y. Chen, J. Gao, A.J. Nozik, M.C. Beard, Science 334 (2011) 1530–1533.
[19] G.S. Paul, J.H. Kim, M.-S. Kim, K. Do, J. Ko, J.-S. Yu, ACS Appl. Mater. Interfaces 4 (2012) 375–381.
[20] M. Samadpour, S. Giménez, P.P. Boix, Q. Shen, M.E. Calvo, N. Taghavinia, A.I. Zad, T. Toyoda, H. Míguez, I. Mora-Seró, Electrochim. Acta 75 (2012) 139–147.
[21] S. Giménez, I. Mora-Seró, L. Macor, N. Guijarro, T. Lana-Villarreal, R. Gómez, L.J. Diguna, Q. Shen, T. Toyoda, J. Bisquert, Nanotechnology 20 (2009) 295204.
[22] I. Mora-Seró, J. Bisquert, J. Phys. Chem. Lett. 1 (2010) 3046–3052.
[23] N. Guijarro, T. Lana-Villarreal, I. Mora-Seró, J. Bisquert, R. Gómez, J. Phys. Chem. C 113 (2009) 4208–4214.
[24] W.W. Yu, L. Qu, W. Guo, X. Peng, Chem. Mater. 15 (2003) 2854–2860.
[25] M. Seol, H. Kim, Y. Tak, K. Yong, Chem. Commun. 46 (2010) 5521–5523.
[26] J. Tian, Q. Zhang, E. Uchaker, Z. Liang, R. Gao, X. Qu, S. Zhang, G. Cao, J. Mater. Chem. A 1 (2013) 6770–6775.
[27] Q. Zhang, G. Chen, Y. Yang, X. Shen, Y. Zhang, C. Li, R. Yu, Y. Luo, D. Li, Q. Meng, Phys. Chem. Chem. Phys. 14 (2012) 6479–6486.
[28] J. Luo, S.K. Karuturi, L. Liu, L.T. Su, A.I.Y. Tok, H.J. Fan, Sci. Rep. 2 (2012) 451.
[29] H.C. van deHulst, Light Scattering by Small Particles, Wiley, New York, 1957.
[30] J. Yu, Q. Li, Z. Shu, Electrochim. Acta 56 (2011) 6293–6298.
[31] J. Yu, J. Fan, B. Cheng, J. Power Sources 196 (2011) 7891–7898.
[32] J. Yu, J. Fan, L. Zhao, Electrochim. Acta 55 (2010) 597–602.
[33] J. Fan, S. Liu, J. Yu, J. Mater. Chem. 22 (2012) 17027–17036.
[34] L. Yang, W.W.-F. Leung, RSC Adv. 3 (2013) 25707–25710.
[35] B. Liu, Y. He, P. Fan, X. Wang, Langmuir 23 (2007) 11266–11272.
[36] S. Ito, P. Chen, P. Comte, M.K. Nazeeruddin, P. Liska, P. Péchy, M. Grätzel, Prog. Photovoltaics 15 (2007) 603–612.
[37] X.-Y. Yu, B.-X. Lei, D.-B. Kuang, C.-Y. Su, Chem. Sci. 2 (2011) 1396–1400.
[38] S.H. Im, H.-J. Kim, S.W. Kim, S.-W. Kim, S.I. Seok, Energy Environ. Sci. 4 (2011) 4181–4186.
[39] S. Hore, P. Nitz, C. Vetter, C. Prahl, M. Niggemann, R. Kern, Chem. Commun. (2005) 2011–2013.
[40] X. Xu, G. Jiang, Q. Wan, J. Shi, G. Xu, L. Miao, Mater. Chem. Phys. 136 (2012) 1060–1066.
[41] T.T.T. Pham, T. Bessho, N. Mathews, S.M. Zakeeruddin, Y.M. Lam, S. Mhaisalkar, M. Grätzel, J. Mater. Chem. 22 (2012) 16201–16204.
[42] G.-J. Ke, H.-Y. Chen, C.-Y. Su, D.-B. Kuang, J. Mater. Chem. A 1 (2013) 13274–13282.
[43] J. Qian, P. Liu, Y. Xiao, Y. Jiang, Y. Cao, X. Ai, H. Yang, Adv. Mater. 21 (2009) 3663–3667.
[44] I. Mora-Seró, S. Giménez, T. Moehl, F. Fabregat-Santiago, T. Lana-Villareal, R. Gómez, J. Bisquert, Nanotechnology 19 (2008) 424007.
[45] I. Robel, V. Subramanian, M. Kuno, P.V. Kamat, J. Am. Chem. Soc. 128 (2006) 2385–2393.
[46] D.-W. Liu, I.-C. Cheng, J.Z. Chen, H.-W. Chen, K.-C. Ho, C.-C. Chiang, Opt. Express 20 (S2) (2012) A168–A176.
[47] J.G. Radich, R. Dwyer, P.V. Kamat, J. Phys. Chem. Lett. 2 (2011) 2453–2460.
[48] L. Mu, C. Liu, J. Jia, X. Zhou, Y. Lin, J. Mater. Chem. A 1 (2013) 8353–8357.
[49] Q. Zhang, X. Guo, X. Huang, S. Huang, D. Li, Y. Luo, Q. Shen, T. Toyoda, Q. Meng, Phys. Chem. Chem. Phys. 13 (2011) 4659–4667.
[50] A. Zaban, M. Greenshtein, J. Bisquert, ChemPhysChem 4 (2003) 859–864.
[51] J. Bisquert, A. Zaban, M. Greenshtein, I. Mora-Seró, J. Am. Chem. Soc. 126 (2004) 13550–13559.